

Total variation regularization of the 3-D gravity inverse problem using a randomized generalized singular value decomposition

Saeed Vatankhah ¹, Rosemary A. Renaut ² and Vahid E. Ardestani ¹

¹ *Institute of Geophysics, University of Tehran, Iran*

² *School of Mathematical and Statistical Sciences, Arizona State University, Tempe, AZ, USA.*

SUMMARY

We present a fast algorithm for the total variation regularization of the 3-D gravity inverse problem. Through imposition of the total variation regularization, subsurface structures presenting with sharp discontinuities are preserved better than when using a conventional minimum-structure inversion. The associated problem formulation for the regularization is non linear but can be solved using an iteratively reweighted least squares algorithm. For small scale problems the regularized least squares problem at each iteration can be solved using the generalized singular value decomposition. This is not feasible for large scale problems. Instead we introduce the use of a randomized generalized singular value decomposition in order to reduce the dimensions of the problem and provide an effective and efficient solution technique. For further efficiency an alternating direction algorithm is used to implement the total variation weighting operator within the iteratively reweighted least squares algorithm. Presented results for synthetic examples demonstrate that the novel randomized decomposition provides good accuracy for reduced computational and memory demands as compared to use of classical approaches.

Key words: Inverse theory; Numerical approximation and analysis; Gravity anomalies and Earth structure; Asia

1 INTRODUCTION

Regularization is imposed in order to find acceptable solutions to the ill-posed and non-unique problem of gravity inversion. Most current regularization techniques minimize a global objective function that consists of a data misfit term and a stabilization term; (Li & Oldenburg 1998; Portniaguine & Zhdanov 1999; Boulanger & Chouteau 2001; Vatankehah et al. 2017a). Generally for potential field inversion the data misfit is measured as a weighted L_2 -norm of the difference between the observed and predicted data of the reconstructed model, (Pilkington 2009). Stabilization aims to both counteract the ill-posedness of the problem so that changes in the model parameters due to small changes in the observed data are controlled, and to impose realistic characteristics on the reconstructed model. Many forms of robust and reliable stabilizations have been used by the geophysical community. L_0 , L_1 and Cauchy norms for the model parameters yield sparse and compact solutions, (Last & Kubik 1983; Portniaguine & Zhdanov 1999; Ajo-Franklin et al. 2007; Pilkington 2009; Vatankehah et al. 2017a). The minimum-structure inversion based on a L_2 measure of the gradient of the model parameters yields a model that is smooth (Li & Oldenburg 1998). Total variation (TV) regularization based on a L_1 norm of the gradient of the model parameters (Bertete-Aguirre et al. 2002; Farquharson 2008) preserves edges in the model and provides a reconstruction of the model that is blocky and non-smooth. While the selection of stabilization for a given data sets depends on an anticipated true representation of the subsurface model and is problem specific, efficient and practical algorithms for large scale problems are desired for all formulations. Here the focus is on the development of a new randomized algorithm for the 3-D linear inversion of gravity data with TV stabilization.

The objective function to be minimized through the stabilization techniques used for geophysical inversion is nonlinear in the model and a solution is typically found using an iteratively reweighted standard Tikhonov least squares (IRLS) formulation. For the TV constraint it is necessary to solve a generalized Tikhonov least squares problem at each iteration. This presents no difficulty for small scale problems; the generalized singular value decomposition (GSVD) can be used to compute the mutual decomposition of the model and stabilization matrices from which a solution is immediate. Furthermore, the use of the GSVD provides a convenient form for the regularization parameter-choice rules, (Xiang & Zou 2013; Chung & Palmer 2015). The approach using the GSVD is not practical for large scale problems, neither in terms of computational costs nor memory demands. Randomized algorithms compute low-rank matrix approximations with reduced memory and computational costs,

(Halko et al. 2011; Xiang & Zou 2013; Voronin et al. 2015; Wei et al. 2016). Random sampling is used to construct a low-dimensional subspace that captures the dominant spectral properties of the original matrix and then, as developed by Wei et al. (2016), a GSVD can be applied to regularize for this dominant spectral space. We demonstrate that applying this randomized GSVD (RGSVD) methodology at each step of the iterative TV regularization provides a fast and efficient algorithm for 3-D gravity inversion that inherits all the properties of TV inversion for small-scale problems. We also show how the weighting matrix at each iteration can be determined and how an alternating direction algorithm can also reduce the memory overhead associated with calculating the GSVD of the projected subproblem at each step of the IRLS.

2 INVERSION METHODOLOGY

Suppose the subsurface is divided into a large number of cells of fixed size but unknown density (Li & Oldenburg 1998; Boulanger & Chouteau 2001). Unknown densities of the cells are stacked in vector $\mathbf{m} \in \mathcal{R}^n$ and measured data on the surface are stacked in $\mathbf{d}_{\text{obs}} \in \mathcal{R}^m$ are related to the densities via the linear relationship

$$\mathbf{d}_{\text{obs}} = G\mathbf{m}, \quad (1)$$

for forward model matrix $G \in \mathcal{R}^{m \times n}$ ($m \ll n$). The aim is to find an acceptable model for the densities that predicts the observed data at the noise level. For gravity inversion, (1) is modified through inclusion of an estimated prior model, \mathbf{m}_{apr} , and a depth weighting matrix, W_{depth} , (Li & Oldenburg 1998; Boulanger & Chouteau 2001) yielding

$$\mathbf{d}_{\text{obs}} - G\mathbf{m}_{\text{apr}} = G\mathbf{m} - G\mathbf{m}_{\text{apr}}. \quad (2)$$

This is replaced first by $G\mathbf{y} = \mathbf{r}$ using $\mathbf{r} = \mathbf{d}_{\text{obs}} - G\mathbf{m}_{\text{apr}}$ and $\mathbf{y} = \mathbf{m} - \mathbf{m}_{\text{apr}}$, and then by incorporating depth weighting, via $\tilde{G} = GW_{\text{depth}}^{-1}$ and $\mathbf{h} = W_{\text{depth}}\mathbf{y}$, further replaced by

$$\mathbf{r} = \tilde{G}\mathbf{h}. \quad (3)$$

Due to the ill-posedness of the problem (3) cannot be solved directly but must be stabilized in order to provide a practically acceptable solution. Using the L_2 -TV regularization methodology \mathbf{h} is obtained by minimizing the objective function (Wohlberg & Rodriguez 2007),

$$P^\alpha(\mathbf{h}) = \|W_{\mathbf{d}}(\tilde{G}\mathbf{h} - \mathbf{r})\|_2^2 + \alpha^2 \|\nabla \mathbf{h}\|_1, \quad (4)$$

in which diagonal weighting matrix $W_{\mathbf{d}}$ approximates the square root of the inverse covariance matrix for the independent noise in the data. Specifically $(W_{\mathbf{d}})_{ii} = 1/\eta_i$ in which η_i is the standard deviation of the noise for the i th datum. Regularization parameter α provides a tradeoff between the

weighted data misfit and the stabilization. The absolute value of the gradient vector, $|\nabla \mathbf{h}|$, is equal to $= \sqrt{(D_x \mathbf{h})^2 + (D_y \mathbf{h})^2 + (D_z \mathbf{h})^2}$ in which D_x , D_y and D_z are the discrete derivative operators in x , y and z -directions, respectively. The derivatives at the centers of the cells are approximated to low order using forward differences with backward differencing at the boundary points, Li & Oldenburg (2000), yielding matrices D_x , D_y and D_z which are square of size $n \times n$. Although (4) is a convex optimization problem with a unique solution, the TV term is not differentiable everywhere with respect to \mathbf{h} and to find a solution it is helpful to rewrite the stabilization term using a weighted L_2 -norm, following Wohlberg & Rodríguez (2007). Given vectors ξ , χ and ψ and a diagonal matrix W_R with entries w_r we have

$$\left\| \begin{pmatrix} W_R & 0 & 0 \\ 0 & W_R & 0 \\ 0 & 0 & W_R \end{pmatrix} \begin{pmatrix} \xi \\ \chi \\ \psi \end{pmatrix} \right\|_2^2 = \sum_r (w_r^2 \xi_r^2 + w_r^2 \chi_r^2 + w_r^2 \psi_r^2) = \sum_r w_r^2 (\sqrt{\xi_r^2 + \chi_r^2 + \psi_r^2})^2. \quad (5)$$

Setting $w_r = (\xi_r^2 + \chi_r^2 + \psi_r^2)^{-1/4}$ we have

$$\left\| \begin{pmatrix} W_R & 0 & 0 \\ 0 & W_R & 0 \\ 0 & 0 & W_R \end{pmatrix} \begin{pmatrix} \xi \\ \chi \\ \psi \end{pmatrix} \right\|_2^2 = \sum_r (\sqrt{\xi_r^2 + \chi_r^2 + \psi_r^2}). \quad (6)$$

Now with $\xi = D_x \mathbf{h}$, $\chi = D_y \mathbf{h}$, $\psi = D_z \mathbf{h}$ and $W_R^{(k)}$ defined to have entries $w_r^{(k)}$ calculated for $\nabla \mathbf{h}$ at iteration $k - 1$ given by $w_r^{(k)} = ((D_x \mathbf{h}^{(k-1)})_r^2 + (D_y \mathbf{h}^{(k-1)})_r^2 + (D_z \mathbf{h}^{(k-1)})_r^2 + \epsilon^2)^{-1/4}$, the TV stabilizer is approximated via

$$\|\nabla \mathbf{h}\|_1^1 = \|\sqrt{(D_x \mathbf{h})^2 + (D_y \mathbf{h})^2 + (D_z \mathbf{h})^2}\|_1^1 \approx \|W^{(k)} D \mathbf{h}\|_2^2, \quad (7)$$

for derivative operator $D = [D_x; D_y; D_z]$. Here, $0 < \epsilon \ll 1$ is added to avoid the possibility of division by zero, and superscript k indicates that matrix W_R is updated using the model parameters of the previous iteration. Hence (4) is rewritten as a general Tikhonov functional

$$P^\alpha(\mathbf{h}) = \|W_d(\tilde{G}\mathbf{h} - \mathbf{r})\|_2^2 + \alpha^2 \|\tilde{D}\mathbf{h}\|_2^2, \quad \tilde{D} = WD, \quad (8)$$

for which the minimum is explicitly expressible as

$$\mathbf{h} = (\tilde{G}^T \tilde{G} + \alpha^2 \tilde{D}^T \tilde{D})^{-1} \tilde{G}^T \tilde{\mathbf{r}}, \quad \tilde{G} = W_d \tilde{G} \quad \text{and} \quad \tilde{\mathbf{r}} = W_d \mathbf{r}. \quad (9)$$

The model update is then

$$\mathbf{m}(\alpha) = \mathbf{m}_{\text{apr}} + W_{\text{depth}}^{-1} \mathbf{h}(\alpha) \quad (10)$$

While the Tikhonov function can be replaced by a standard form Tikhonov function, i.e. with regularization term $\|\mathbf{h}\|^2$, when \tilde{D} is easily invertible, e.g. when diagonal, the form of \tilde{D} in this case makes that transformation prohibitive for cost and we must solve using the general form.

We show the iterative process for the solution in Algorithm 2. It should be noted that the iteration process terminates when solution satisfies the noise level or a predefined maximum number of iterations is reached (Boulangier & Chouteau 2001). Furthermore, the positivity constraint $[\rho_{\min}, \rho_{\max}]$ is imposed at each iteration. If at any iteration a density value falls outside these predefined density bounds, the value is projected back to the nearest bound value (Boulangier & Chouteau 2001).

For small-scale problems in which the dimensions of \tilde{G} , and consequently \tilde{D} , are small, the the solution $\mathbf{h}(\alpha)$ is found at minimal cost using the GSVD of the matrix pair $[\tilde{G}, \tilde{D}]$ as it is shown in Appendix A (Aster et al. 2013; Vatankhah et al. 2014). Furthermore, given the GSVD the regularization parameter may be estimated cheaply using standard parameter-choice techniques (Xiang & Zou 2013; Chung & Palmer 2015). But for large scale problems it is not practical to calculate the GSVD at each iteration, both with respect to computational cost and memory demands. Instead the size of the original large problem can be reduced greatly using a randomization technique which provides the GSVD in a more feasible and efficient manner. The solution of reduced system still is a good approximation of the original system (Halko et al. 2011; Xiang & Zou 2013; Voronin et al. 2015; Xiang & Zou 2015; Wei et al. 2016). Here, we use the Randomized GSVD (RGSVD) algorithm developed by Wei et al. (2016) for under-determined problems, in which the mutual decomposition of the matrix pair $[\tilde{G}, \tilde{D}]$ is approximated by

$$\tilde{G} \approx U\Lambda Z, \quad \tilde{D} = VMZ, \quad U \in \mathcal{R}^{m \times q}, V \in \mathcal{R}^{3n \times q}, \Lambda \in \mathcal{R}^{q \times q}, M \in \mathcal{R}^{q \times q}, Z \in \mathcal{R}^{q \times n}. \quad (11)$$

Algorithm 1 RGSVD algorithm. Given matrices $\tilde{G} \in \mathcal{R}^{m \times n} (m \leq n)$ and $\tilde{D} \in \mathcal{R}^{3n \times n}$, a target matrix rank q and a small constant oversampling parameter p satisfying $q + p = l \ll m$, compute an approximate GSVD of $[\tilde{G}, \tilde{D}]$: $\tilde{G} \approx U\Lambda Z$, $\tilde{D} = VMZ$ with $U \in \mathcal{R}^{m \times q}$, $V \in \mathcal{R}^{3n \times q}$, $\Lambda \in \mathcal{R}^{q \times q}$, $M \in \mathcal{R}^{q \times q}$ and $Z \in \mathcal{R}^{q \times n}$.

- 1: Generate a Gaussian random matrix $\Omega \in \mathcal{R}^{l \times m}$.
 - 2: Form the matrix $Y = \Omega \tilde{G} \in \mathcal{R}^{l \times n}$.
 - 3: Compute orthonormal matrix $Q \in \mathcal{R}^{n \times l}$ via QR factorization $Y^T = QR$.
 - 4: Set $Q = Q(:, 1 : q)$ and form the matrices $B_1 = \tilde{G}Q \in \mathcal{R}^{m \times q}$ and $B_2 = \tilde{D}Q \in \mathcal{R}^{3n \times q}$.
 - 5: Compute the GSVD of $[B_1, B_2]$: $\begin{bmatrix} B_1 \\ B_2 \end{bmatrix} = \begin{bmatrix} U \\ V \end{bmatrix} \begin{bmatrix} \Lambda \\ M \end{bmatrix} X^T$, using $[U, V, X, \Lambda, M] = \text{gsvd}(B_1, B_2, 0)$.
 - 6: Form the matrix $Z = X^T Q^T \in \mathcal{R}^{q \times n}$.
-

The steps of the algorithm are given in Algorithm 1. Steps 1 to 3 are used to form matrix Q which approximates the range of \tilde{G}^T . At step 4, \tilde{G} is projected into a lower dimensional matrix B_1 , for which B_1 provides information on the range of \tilde{G} . The same projection is applied to matrix \tilde{D} .

In step 5, an economy-sized GSVD is computed for the matrix pair $[B_1, B_2]$. Parameter q balances the accuracy and efficiency of the Algorithm 1 and determines the dimension of the subspace for the projected problem. When q is small, this methodology is very effective and leads to a fast GSVD computation. Simultaneously, the parameter q has to be selected large enough to capture the dominant spectral properties of the original problem with the aim that the solution obtained using the RGSVD is close to the solution that would be obtained using the GSVD.

For any GSVD decomposition (11), including that obtained via Algorithm 1, $\mathbf{h}(\alpha)$ of (9) is given by

$$\mathbf{h}(\alpha) = (Z^T \Lambda^T U^T U \Lambda Z + \alpha^2 Z^T M^T V^T V M Z)^{-1} Z^T \Lambda^T U^T \tilde{\mathbf{r}}, \quad (12)$$

which simplifies to, (Aster et al. 2013; Vatankhah et al. 2014),

$$\mathbf{h}(\alpha) = \sum_{i=1}^q \frac{\gamma_i^2}{\gamma_i^2 + \alpha^2} \frac{\mathbf{u}_i^T \tilde{\mathbf{r}}}{\lambda_i} (Z^{-1})_i. \quad (13)$$

Here γ_i is the i th generalized singular value, see Appendix A, and Z^{-1} is the Moore-Penrose inverse of Z (Wei et al. 2016). Incorporating this single step of the RGSVD within the TV algorithm, yields the iteratively reweighted TVRGSVD algorithm given in Algorithm 2. Note here that the steps 1-3 and the calculation of B_1 in step 4 in Algorithm 1 are the same for all TV iterations and thus outside the loop in Algorithm 2. At each iteration k , the matrices W , \tilde{D} and B_2 are updated, and the GSVD is determined for the matrix pair $[B_1, B_2^{(k)}]$. We should note here that it is immediate to use the minimum gradient support (MGS) stabilizer introduced by Portniaguine & Zhdanov (1999) in Algorithm 2 via replacing $(-1/4)$ in W_R with $(-1/2)$ and keeping all other parameters are kept fixed.

2.0.1 An Alternating Direction Algorithm

Step 9 of Algorithm 2 requires the economy GSVD decomposition in which matrix $B_2^{(k)}$ is of size $3n \times q$. For a large scale problem the computational cost and memory demands with the calculation of the GSVD limits the size of the problem that can be solved. We therefore turn to an alternative approach for large scale three dimensional problems and adopt the use of an Alternating Direction (AD) strategy, in which to handle the large scale problem requiring derivatives in greater than two dimensions we split the problem into pieces handling each direction one after the other. This is a technique that has been in the literature for some time for handling the solution of large scale partial differential equations, most notably through the alternating direction implicit method (Peaceman & Rachford 1955). Matrix $D^{(k)}$ generated via steps 16 and 17 of Algorithm 2 can be changed without changing the other steps of the algorithm. For the AD algorithm we may therefore alternate over $D^{(k)} = W_{R_x}^{(k)} D_x$, $W_{R_y}^{(k)} D_y$ or $W_{R_z}^{(k)} D_z$, dependent on $(k \bmod 3) = 0, 1, \text{ or } 2$, respectively. Then

Algorithm 2 Iterative TV inversion algorithm using randomized GSVD**Input:** $\mathbf{d}_{\text{obs}}, \mathbf{m}_{\text{apr}}, G, W_{\mathbf{d}}, W_{\text{depth}}, D_x, D_y, D_z, q, \epsilon > 0, \rho_{\min}, \rho_{\max}, K_{\max}$

- 1: Initialize $\mathbf{m}^{(0)} = \mathbf{m}_{\text{apr}}, W^{(1)} = I, D = [D_x; D_y; D_z], \tilde{D}^{(1)} = D, k = 1$
- 2: Calculate $\tilde{G} = W_{\mathbf{d}} G W_{\text{depth}}^{-1}, \tilde{\mathbf{r}}^{(1)} = W_{\mathbf{d}}(\mathbf{d}_{\text{obs}} - G\mathbf{m}_{\text{apr}})$
- 3: Generate a Gaussian random matrix $\Omega \in \mathcal{R}^{l \times m}$.
- 4: Compute matrix $Y = \Omega \tilde{G} \in \mathcal{R}^{l \times n}$.
- 5: Compute orthonormal matrix $Q \in \mathcal{R}^{n \times l}$ via QR factorization $Y^T = QR$.
- 6: Set $Q = Q(:, 1 : q)$ and form the the matrix $B_1 = \tilde{G}Q \in \mathcal{R}^{m \times q}$.
- 7: **while** Not converged, noise level not satisfied, and $k < K_{\max}$ **do**
- 8: Form the matrix $B_2 = \tilde{D}^{(k)}Q \in \mathcal{R}^{3n \times q}$.
- 9: Compute the GSVD of $\{B_1, B_2\}: [U, V, X, \Lambda, M] = \text{gsvd}(B_1, B_2, 0)$.
- 10: Form the matrix $Z = X^T Q^T \in \mathcal{R}^{q \times n}$.
- 11: Estimate $\alpha^{(k)}$ using (15)
- 12: Set $\mathbf{h}^{(k)} = \sum_{i=1}^q \frac{\gamma_i^2}{\gamma_i^2 + (\alpha^{(k)})^2} \frac{\mathbf{u}_i^T \tilde{\mathbf{r}}^{(k)}}{\lambda_i} (Z^{-1})_i$.
- 13: Set $\mathbf{m}^{(k)} = \mathbf{m}^{(k-1)} + (W_{\text{depth}})^{-1} \mathbf{h}^{(k)}$.
- 14: Impose constraint conditions on $\mathbf{m}^{(k)}$ to force $\rho_{\min} \leq \mathbf{m}^{(k)} \leq \rho_{\max}$.
- 15: Test convergence and exit loop if converged.
- 16: Calculate $W_{\mathbf{R}}^{(k+1)} = \text{diag}(((D_x \mathbf{h}^{(k)})^2 + (D_y \mathbf{h}^{(k)})^2 + (D_z \mathbf{h}^{(k)})^2 + \epsilon^2)^{-1/4})$ and set $W^{(k+1)} = \text{diag}(W_{\mathbf{R}}^{(k+1)}; W_{\mathbf{R}}^{(k+1)}; W_{\mathbf{R}}^{(k+1)})$.
- 17: Set $\tilde{\mathbf{r}}^{(k+1)} = W_{\mathbf{d}}(\mathbf{d}_{\text{obs}} - G\mathbf{m}^{(k)}), \tilde{D}^{(k+1)} = W^{(k+1)}D$,
- 18: $k = k + 1$
- 19: **end while**

Output: Solution $\rho = \mathbf{m}^{(k)}$. $K = k$.

$B_2^{(k)}$ is only of size $n \times n$, yielding reduced memory demands for calculating the GSVD. We note that D is also initialized consistently. The AD approach amounts to apply the edge preserving algorithm in each direction independently and cycling over all directions. Practically, we also find that there is nothing to be gained by requiring that the derivative matrices are square, and following (Hansen 2007) ignore the derivatives at the boundaries. For a one dimensional problem this amounts to taking matrix D_x of size $(n - 1) \times n$ for a line with n points. Thus dependent on $k \bmod 3$ we have a weighting matrix of size $p_x \times p_x, p_y \times p_y$ or $p_z \times p_z$ for matrices D_x, D_y and D_z of sizes $p_x \times n, p_y \times n$ and $p_z \times n$, respectively, and where p_x, p_y and p_z (all less than n) depend on the number of boundary points in each direction. Matrix $B_2^{(k)}$ is thus reduced in size and the GSVD calculation is more efficient at each step. Furthermore, we find that rather than calculating the relevant weight matrix $W_{\mathbf{R}}$ for the given dimension we actually form the weighted entry that leads to approximation of the relevant component

of the gradient vector for all three dimensions, thus realistically approximating the gradient as given in (5). For the presented results we will use the AD version of Algorithm 2, noting that this is not necessary for the smaller problems, but is generally more efficient and reliable for the larger three dimensional problem formulations.

2.1 Estimation of the Regularization Parameter α

As presented to this point we have assumed a known value for the regularization parameter α . Practically we wish to find α dynamically to appropriately regularize at each step of the iteration so as to recognize that the conditioning of the problem changes with the iteration. Here we use the method of unbiased predictive risk estimation (UPRE) which we have found to be robust in our earlier work (Renaut et al. 2017; Vatankhah et al. 2015; Vatankhah et al. 2017a). The method, which goes back to Mallows (1973), requires some knowledge of the noise level in the data and was carefully developed in Vogel (2002) for the standard Tikhonov functional. The method was further extended for use with TV regularization by Lin et al. (2010). Defining the residual $R(\mathbf{h}(\alpha)) = \tilde{\mathbf{G}}\mathbf{h}(\alpha) - \tilde{\mathbf{r}}$ and influence matrix $H_{TV,\alpha} = \tilde{\mathbf{G}}(\tilde{\mathbf{G}}^T\tilde{\mathbf{G}} + \alpha^2\tilde{\mathbf{D}}^T\tilde{\mathbf{D}})^{-1}\tilde{\mathbf{G}}^T$, the optimal parameter α is the minimizer of

$$U(\alpha) = \|R(\mathbf{h}(\alpha))\|_2^2 + 2\text{trace}(H_{TV,\alpha}) - m, \quad (14)$$

which is given in terms of the GSVD by

$$U(\alpha) = \sum_{i=1}^q \left(\frac{1}{\gamma_i^2\alpha^{-2} + 1} \right)^2 (\mathbf{u}_i^T \tilde{\mathbf{r}})^2 + 2 \left(\sum_{i=1}^q \frac{\gamma_i^2}{\gamma_i^2 + \alpha^2} \right) - q. \quad (15)$$

Typically α_{opt} is found by evaluating (15) on a range of α , between minimum and maximum γ_i , and then that α which minimizes the function is selected as α_{opt} .

3 SYNTHETIC EXAMPLES

3.1 Model consisting of two dipping dikes

As a first example, we use a complex model that consists of two embedded dipping dikes of different sizes and dipping in opposite directions but with the same density contrast 1 g cm^{-3} , Fig. 1. Gravity data, $\mathbf{d}_{\text{exact}}$, is generated on the surface for a grid of $30 \times 30 = 900$ points with grid spacing 50 m. Gaussian noise with standard deviation $(0.02 (\mathbf{d}_{\text{exact}})_i + 0.002 \|\mathbf{d}_{\text{exact}}\|)$ is added to each datum. Example noisy data, \mathbf{d}_{obs} , is illustrated in Fig. 2. Inversion is performed for the subsurface volume of 9000 cubes of size 50 m in each dimension using the matrix $\tilde{\mathbf{G}}$ of size 900×9000 . Use of this relatively small model permits examination of the inversion methodology with respect to different parameter choices and provides the framework to be used for more realistic larger models. All computations are performed on a desktop computer with Intel Core i7-4790 CPU 3.6GHz processor and 16 GB RAM.

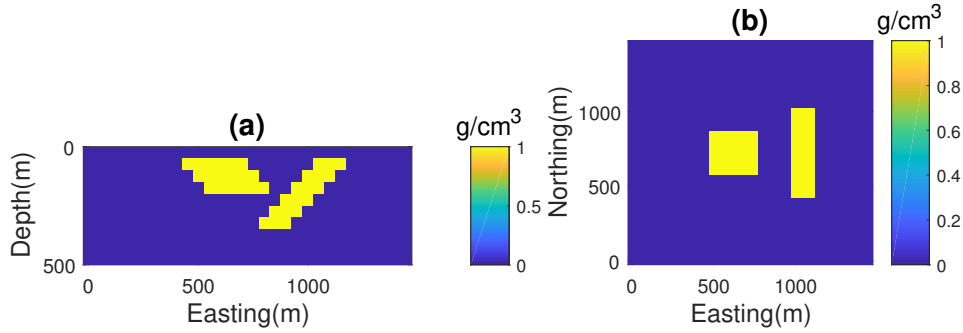


Figure 1. A model that consists of two dikes dipping in opposite directions. (a) Cross-section at northing = 725 m; (b) Plane-section at depth = 100 m.

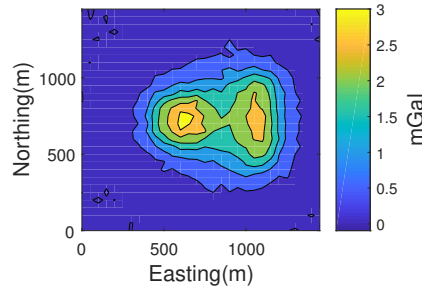


Figure 2. The gravity anomaly produced by the model shown in Fig. 1 and contaminated by Gaussian noise.

Table 1. Parameters and results for Algorithm 2 applied to the small scale dipping dikes model. The number of iterations is K , $\alpha^{(K)}$ is the final regularization parameter, $RE^{(K)} = \frac{\|\mathbf{m}_{\text{exact}} - \mathbf{m}^{(K)}\|_2}{\|\mathbf{m}_{\text{exact}}\|_2}$ is the relative error of the reconstructed model at iteration K . The final χ^2_{computed} is also reported.

Input Parameters					Results				
\mathbf{m}_{apr}	$\rho_{\text{min}} \text{ (g cm}^{-3}\text{)}$	$\rho_{\text{max}} \text{ (g cm}^{-3}\text{)}$	K_{max}	q	$RE^{(K)}$	$\alpha^{(K)}$	K	χ^2_{computed}	Time (s)
$\mathbf{0}$	0	1	200						
				100	0.7745	26.63	200	3978.9	494
				300	0.7143	41.62	174	942.4	595
				500	0.7244	51.62	49	942.2	249
$\mathbf{0}$	0	1	50	300	0.7308	38.01	50	1165.7	165
$\mathbf{0}$	0	2	200	500	0.7257	31.60	49	941.6	227
$\neq \mathbf{0}$	0	1	200	500	0.7076	76.74	200	1952.6	972

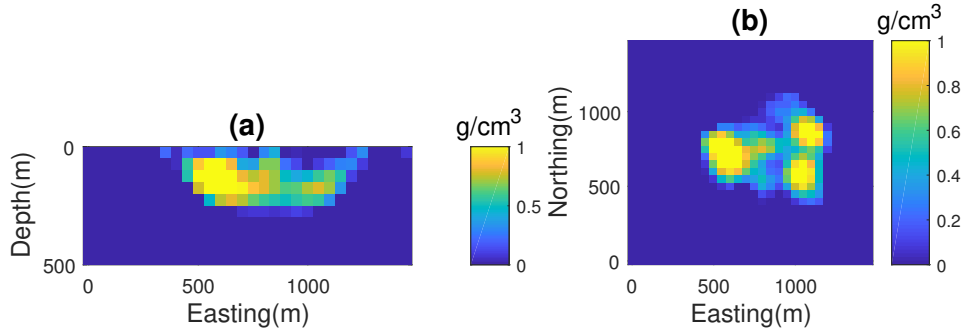


Figure 3. The reconstructed model for data in Fig. 2 using Algorithm 2 with $q = 100$. (a) Cross-section at northing = 725 m; (b) Plane-section at depth = 100 m.

The parameters of the inversion needed for Algorithm 2, and the results, are detailed for each example in Table 1. These are the maximum number of iterations for the inversion K_{\max} , the bound constraints for the model ρ_{\min} and ρ_{\max} , the initial data \mathbf{m}_{apr} and the choice for q . Further the inversion terminates if $\chi_{\text{computed}}^2 = \|\mathbf{W}_{\mathbf{d}}(\mathbf{d}_{\text{obs}} - \mathbf{d}_{\text{pre}}^{(K)})\|_2^2 \leq m + \sqrt{2m} = 942.4$ is satisfied for iteration $K < K_{\max}$. The results for different choices of q , but all other parameters the same, are illustrated in Figs. 3, 4 and 5, respectively. With $q = 100$ two dipping structures are recovered but the iteration has not converged by $K = 200$, and both the relative error and χ_{computed}^2 are large. With $q = 300$ and 500 better reconstructions of the dikes are achieved although the extension of the left dike is overestimated. While the errors are nearly the same, the inversions terminate at $K = 174$ and $K = 49$ for $q = 300$ and $q = 500$, respectively. This leads to low computational time when using $q = 500$ as compared with the other two cases, see Table 1. We should note here that for all three cases the relative error decreases rapidly for the early iterations, after which there is little change in the model between iterations. For example the result for $q = 300$ at iteration $K = 50$, as illustrated in Fig. 6 and detailed in Table 1, is acceptable and is achieved with a substantial reduction in the computational time.

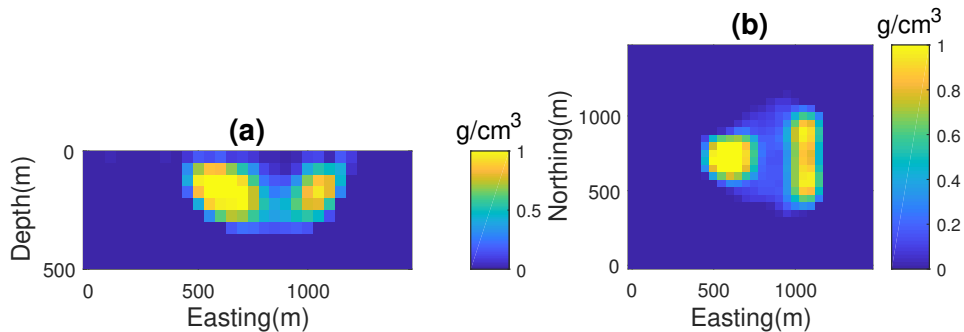


Figure 4. The reconstructed model for data in Fig. 2 using Algorithm 2 with $q = 300$. (a) Cross-section at northing = 725 m; (b) Plane-section at depth = 100 m.

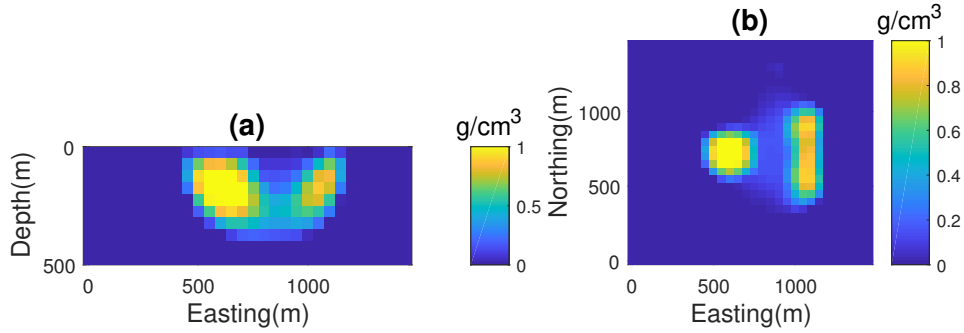


Figure 5. The reconstructed model for data in Fig. 2 using Algorithm 2 with $q = 500$. (a) Cross-section at northing = 725 m; (b) Plane-section at depth = 100 m.

As compared to inversion using the L_2 -norm of the gradient of the model parameters, see for example Li & Oldenburg (1996), or conventional minimum structure inversion, the results obtained using Algorithm 2 provide a subsurface model that is not smooth. Further, as compared with L_0 and L_1 norms applied for the model parameters, see for example (Last & Kubik 1983; Portniaguine & Zhdanov 1999; Vatankhah et al. 2017a), the TV inversion does not yield a model that is sparse or compact. On the other hand, the TV inversion is far less dependent on correct specification of the model constraints. This is illustrated in Fig. 7, which is the same case as Fig. 5, but with $\rho_{\max} = 2 \text{ g cm}^{-3}$, and demonstrates that the approach is generally robust. Finally, to contrast with the algorithm presented in Bertete-Aguirre et al. (2002) the results in Fig 8(b) are for an alternative choice for \mathbf{m}_{apr} , illustrated in Fig. 8(a), and $q = 500$ which is consistent with the approach in Bertete-Aguirre et al. (2002). Here \mathbf{m}_{apr} is obtained by taking the true model with the addition of Gaussian noise with a standard deviation of $(0.05 \mathbf{m}_{\text{true}} + 0.02 \|\mathbf{m}_{\text{true}}\|)$. Not surprisingly the reconstructed density model is more focused and is closer to the true model. The computed value for χ^2_{computed} is, however, larger than the specified value and the algorithm terminates at K_{\max} . This occurs due to the appearance of an incorrect density

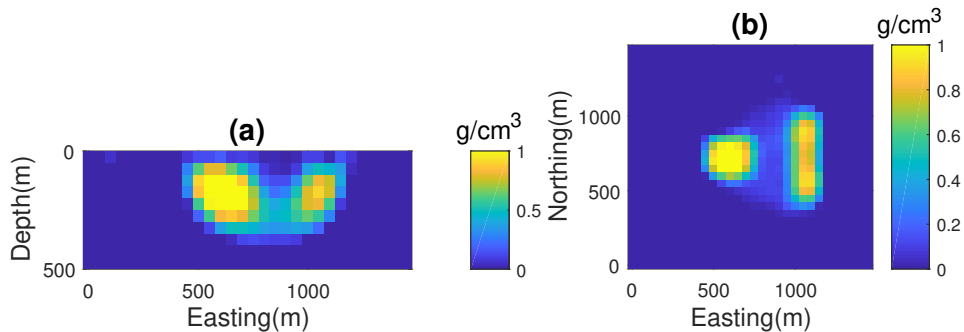


Figure 6. The reconstructed model for data in Fig. 2 using Algorithm 2 with $q = 300$ at $K = 50$. (a) Cross-section at northing = 725 m; (b) Plane-section at depth = 100 m.

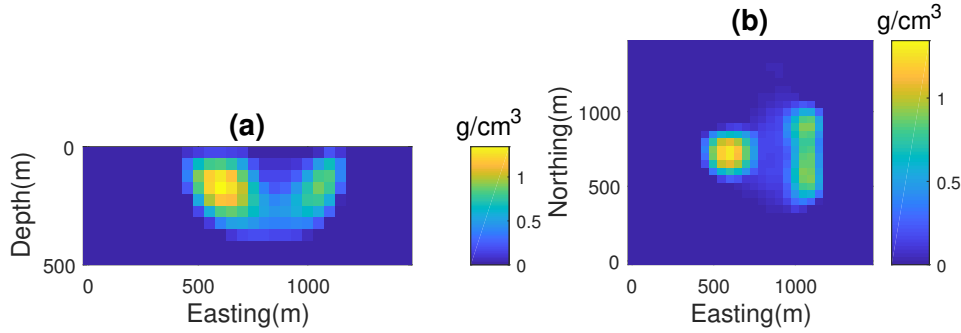


Figure 7. The reconstructed model for data in Fig. 2 using Algorithm 2 with $q = 500$ when uncorrected upper density bound $\rho_{\max} = 2 \text{ g cm}^{-3}$ is selected. (a) Cross-section at northing = 725 m; (b) Plane-section at depth = 100 m.

distribution in the first layer of the subsurface. Together, these results demonstrate that the TVRGSVD technique is successful and offers a good option for the solution of larger scale models.

3.2 Model of multiple bodies

We now consider a more complex and larger model that consists of six bodies with various geometries, sizes, depths and densities, as illustrated in Fig. 9, and is further detailed in Vatankhah et al (2017a). The surface gravity data are calculated on a 100×60 grid with 100 m spacing. Gaussian noise with standard deviation of $(0.02 (\mathbf{d}_{\text{exact}})_i + 0.001 \|\mathbf{d}_{\text{exact}}\|)$ is added to each datum, giving the noisy data set as shown in Fig. 10. The subsurface is divided into $100 \times 60 \times 10 = 60000$ cubes with sizes 100 m in each dimension. For the inversion we use Algorithm 2 with $\mathbf{m}_{\text{apr}} = \mathbf{0}$, $\rho_{\min} = 0 \text{ g cm}^{-3}$, $\rho_{\max} = 1 \text{ g cm}^{-3}$ and $K_{\max} = 50$. We perform the inversion for three values of q , 500, 1000 and 2000, and report the results in Table 2. The reconstruction with $q = 500$ is less satisfactory than that achieved with larger q and the iterations terminate at K_{\max} with a large value of χ_{computed}^2 . The results with $q = 1000$ and $q = 2000$ have similar relative errors, but the computational cost is much reduced

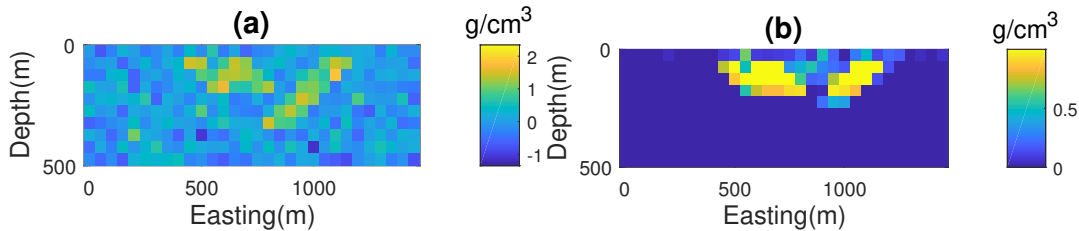


Figure 8. (a) The initial model which generated by adding Gaussian noise with standard deviation of $(0.05 \mathbf{m}_{\text{true}} + 0.02 \|\mathbf{m}_{\text{true}}\|)$ to the true model. (b) The reconstructed model for data in Fig. 2 using Algorithm 2 with $q = 500$ when model shown in Fig. 8(a) is used as \mathbf{m}_{apr} .

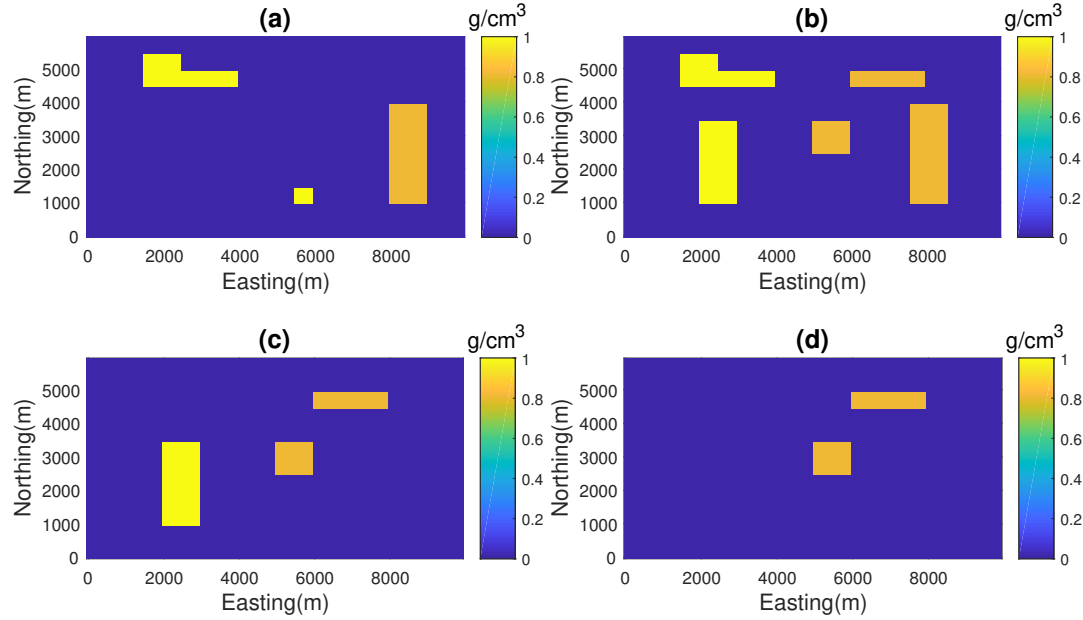


Figure 9. Model consists of six bodies with various geometries and sizes embedded in a homogeneous background. Bodies have the densities 1 g cm^{-3} and 0.8 g cm^{-3} . (a) Plane-section at depth = 100 m; (b) Plane-section at depth = 300 m; (c) Plane-section at depth = 500 m; (d) Plane-section at depth = 700 m.

using $q = 1000$; although the desired χ^2_{computed} is not achieved the result is close and acceptable. The reconstructed model and associated gravity response, using $q = 1000$, are illustrated in Figs. 11 and 12, respectively. While the maximum depths of the anomalies are overestimated, the horizontal borders are reconstructed accurately. These two examples suggest that $q > m/6$ is suitable for Algorithm 2, which confirms our previous conclusions when using the randomized SVD, see Vatankhah et al. (2017b). We should note that as compared to the case in which the standard Tikhonov functional can be used, see such results with the focusing inversion in Vatankhah et al. (2017a; 2017b), the computational cost here is much higher.

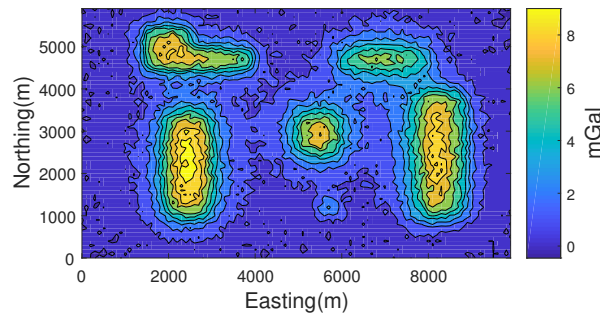


Figure 10. The gravity anomaly produced by the multiple model shown in Fig. 9 and contaminated by Gaussian noise.

Table 2. The results of the inversion for the multiple bodies example using Algorithm 2.

Input Parameters					Results					
\mathbf{m}_{apr}	$\rho_{\text{min}} \text{ (g cm}^{-3}\text{)}$	$\rho_{\text{max}} \text{ (g cm}^{-3}\text{)}$	K_{max}	q	$RE^{(K)}$	$\alpha^{(K)}$	K	χ_{computed}^2	Time (s)	
0	0	1	50	500	0.6710	15.31	50	11719.2	6014	
0	0	1	50	1000	0.6451	18.02	50	7324.0	7262	
0	0	1	50	2000	0.6452	18.79	44	6103.4	10666	

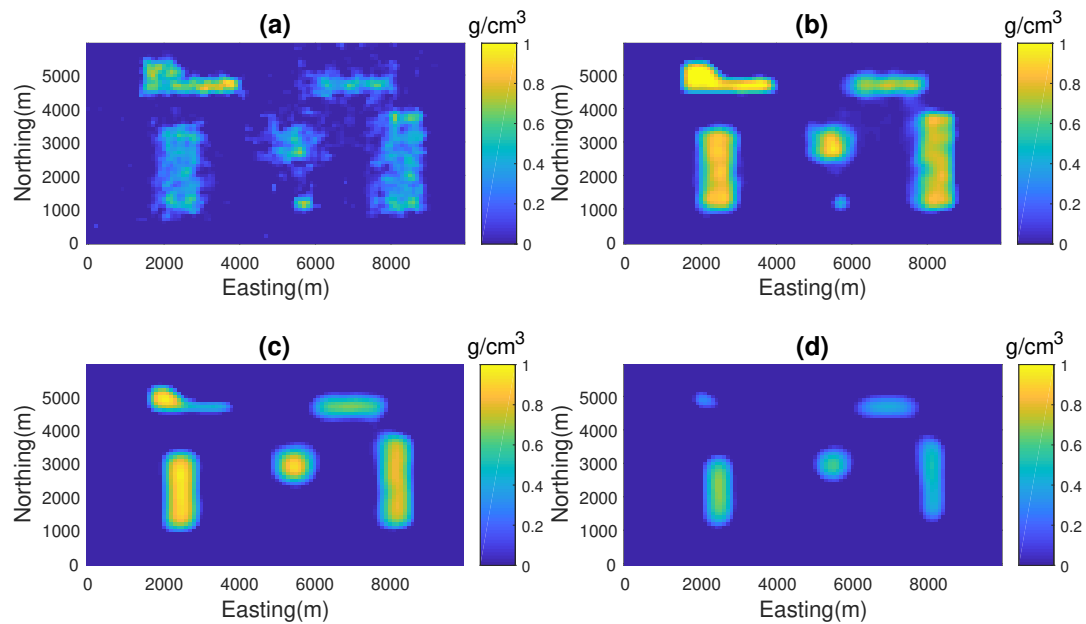
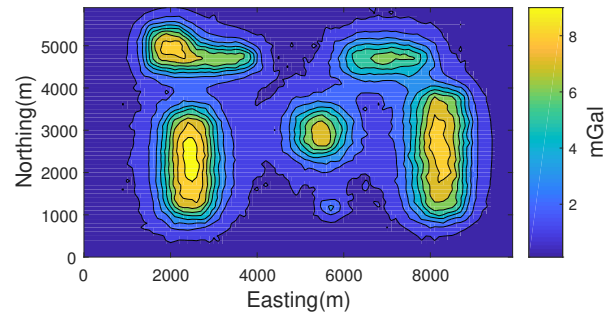
**Figure 11.** The reconstructed model for data in Fig. 10 using Algorithm 2 with $q = 1000$. (a) Plane-section at depth = 100 m; (b) Plane-section at depth = 300 m; (c) Plane-section at depth = 500 m; (d) Plane-section at depth = 700 m.**Figure 12.** The gravity anomaly produced by the reconstructed model shown in Fig. 11.

Table 3. The results of the inversion for the data presented in Fig. 13(a) using Algorithm 2.

Input Parameters					Results			
\mathbf{m}_{apr}	$\rho_{\text{min}} \text{ (g cm}^{-3}\text{)}$	$\rho_{\text{max}} \text{ (g cm}^{-3}\text{)}$	K_{max}	q	$\alpha^{(K)}$	K	χ_{computed}^2	Time (s)
0	0	0.3	100	500	102.48	38	2453.9	1533

4 REAL DATA

We use the gravity data from the Goiás Alkaline Province (GAP) of the central region of Brazil. The GAP is a result of mafic-alkaline magmatism that occurred in the Late Cretaceous and includes mafic-ultramafic alkaline complexes in the northern portion, subvolcanic alkaline intrusions in the central region and volcanic products to the south with several dikes throughout the area (Dutra et al. 2012). We select a region from the northern part of GAP in which Morro do Engenho Complex (ME) outcrops and another intrusive body, A2, is completely covered by Quaternary sediments (Dutra & Marangoni 2009). The data was digitized carefully from Fig. 3 in Dutra & Marangoni (2009) and re-gridded into $45 \times 53 = 2385$ data points with spacing 1 km, Fig. 13(a). For these data, the result of the smooth inversion using Li & Oldenburg (1998) algorithm was presented in Dutra & Marangoni (2009) and Dutra et al. (2012). Furthermore, the result of focusing inversion based on L_1 -norm stabilizer is available in Vatankhah et al. (2017b). The results using the TV inversion presented here can therefore be compared with the inversions using both aforementioned algorithms.

For the inversion we divide the subsurface into $45 \times 53 \times 14 = 33390$ rectangular 1– km prisms. The density bounds $\rho_{\text{min}} = 0 \text{ g cm}^{-3}$ and $\rho_{\text{max}} = 0.3 \text{ g cm}^{-3}$ are selected based on geological information from Dutra & Marangoni (2009). Algorithm 2 was implemented with $q = 500$ and $K_{\text{max}} = 100$. The results of the inversion are presented in Table 3, with the illustration of the predicted data due to the reconstructed model in Fig. 13(b) and the reconstructed model in Fig. 14. As compared to the smooth estimate of the subsurface shown in Dutra & Marangoni (2009), the obtained subsurface is blocky and non-smooth. The subsurface is also not as sparse as that obtained by the focusing inversion in Vatankhah et al. (2017b). The ME and A2 bodies extend up to maximum 12 km and 8 km, respectively. Unlike the result obtained using the focusing inversion, for the TV inversion the connection between ME and A2 at depths 4 km to 7 km is not strong. We should note that the computational time for the focusing inversion presented in Vatankhah et al. (2017b) is much smaller than for the TV algorithm presented here.

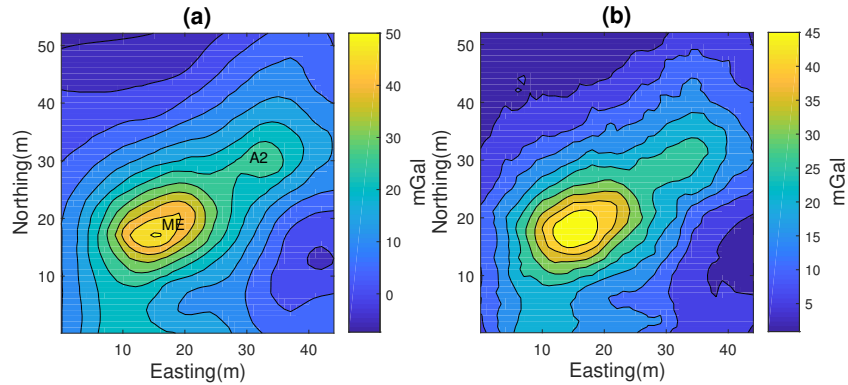


Figure 13. (a) Residual gravity data over the Morro do Engenho complex digitized from Dutra & Marangoni (2009); (b) The response of the reconstructed model shown in Fig. 14.

5 CONCLUSIONS

We developed an algorithm for total variation regularization applied to the 3-D gravity inverse problem. The presented algorithm provides a non-smooth and blocky image of the subsurface which may be useful when discontinuity of the subsurface is anticipated. Using the randomized generalized singular value decomposition, we have demonstrated that moderate-scale problems can be solved in a reasonable computational time. This seems to be the first use of the TV regularization using the RGSVD for gravity inversion. Our presented results use an Alternating Direction implementation to further

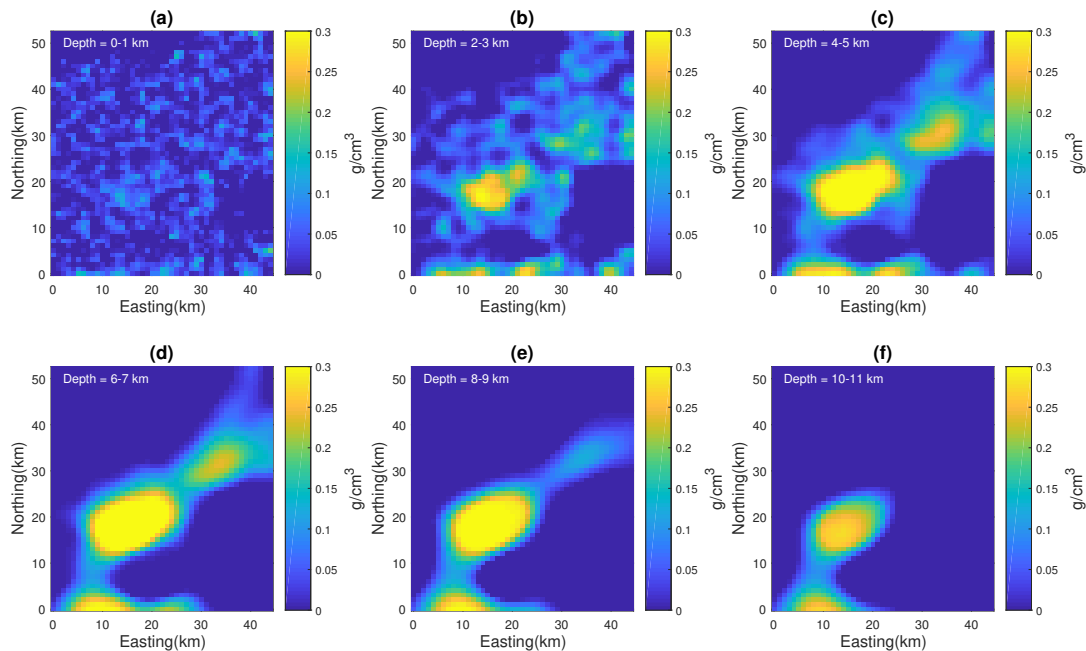


Figure 14. The plane-sections of the reconstructed model for the data in Fig. 13(a) using Algorithm 2 with $q = 400$. The sections are at the depths specified in the figures.

improve the efficiency and reduce the memory demands of the problem. The results show that there is less sensitivity to the provision of good bounds for the density values, and thus the TV may have a role to play for moderate scale problems where limited information on subsurface model parameters is available. It was of interest to investigate the 3-D algorithm developed here in view of the results of Bertete-Aguirre et al. (2002) which advocated TV regularization in the context of 2-D gravity inversion. We obtained results that are comparable with the simulations presented in Bertete-Aguirre et al. (2002) but here for much larger problems. In our simulations we have found that the computational time is much larger than that required for the focusing algorithm presented in Vatankhah et al. (2017a; 2017b). Because it is not possible to transform the TV regularization to standard Tikhonov form, the much more expensive GSVD algorithm has to be used in place of the SVD that can be utilized for the focusing inversion presented in Vatankhah et al. (2017b). On the other hand, the advantage of the TV inversion as compared to the focusing inversion is the lesser dependence on the density constraints and the generation of a subsurface which is not as smooth and admits discontinuities. The impact of the algorithm was illustrated for the inversion of real gravity data from the Morro do Engenho complex in central Brazil.

ACKNOWLEDGMENTS

REFERENCES

- Ajo-Franklin, J. B., Minsley, B. J. & Daley, T. M., 2007. Applying compactness constraints to differential traveltimes tomography, *Geophysics*, **72**(4), R67-R75.
- Aster, R. C., Borchers, B., & Thurber, C. C., 2013, *Parameter Estimation and Inverse Problems*, 2nd ed., Elsevier.
- Bertete-Aguirre, H., Cherkaev, E. & Oristaglio, M., 2002. Non-smooth gravity problem with total variation penalization functional, *Geophys. J. Int.*, **149**, 499-507.
- Boulanger, O. & Chouteau, M., 2001. Constraint in 3D gravity inversion, *Geophysical prospecting*, **49**, 265-280.
- Chung, J. & Palmer, K., 2015. A hybrid LSMR algorithm for large-scale Tikhonov regularization, *SIAM J. Sci. Comput.*, **37** (5), S562-S580.
- Dutra, A. C. & Marangoni, Y. R., 2009. Gravity and magnetic 3D inversion of Morro do Engenho complex, Central Brazil, *Journal of South American Earth Sciences*, **28**, 193-203.
- Dutra, A. C., Marangoni, Y. R. & Junqueira-Brod, T. C., 2012. Investigation of the Goiás Alkaline Province, Central Brazil: Application of gravity and magnetic methods, *Journal of South American Earth Sciences*, **33**, 43-55.
- Farquharson, C. G., 2008. Constructing piecewise-constant models in multidimensional minimum-structure inversions, *Geophysics*, **73**(1), K1-K9.

- Halko, N., Martinsson, P. G., & Tropp, J. A., 2011. Finding structure with randomness: Probabilistic algorithms for constructing approximate matrix decompositions, *SIAM Rev*, **53(2)**, 217-288.
- Hansen, P. C., 2007. *Regularization Tools: A Matlab Package for Analysis and Solution of Discrete Ill-Posed Problems Version 4.1 for Matlab 7.3*, Numerical Algorithms, **46**, 189-194.
- Last, B. J. & Kubik, K., 1983. Compact gravity inversion, *Geophysics*, **48**, 713-721.
- Li, Y. & Oldenburg, D. W., 1996. 3-D inversion of magnetic data, *Geophysics*, **61**, 394-408.
- Li, Y. & Oldenburg, D. W., 1998. 3-D inversion of gravity data, *Geophysics*, **63**, 109-119.
- Li, Y. & Oldenburg, D. W., 2000. Incorporating geologic dip information into geophysical inversions, *Geophysics*, **65**, 148-157.
- Lin, Y., Wohlberg, B. & Guo, H., 2010. UPRE method for total variation parameter selection, *Signal Processing*, **90**, 2546-2551.
- Mallows, C. L., 1973, Some comments on C_p , *Technometrics*, **4(15)**, 661-675.
- Peaceman, D., & Rachford, J. H. H, 1955, The numerical solution of parabolic and elliptic differential equations, *J. Soc. Indust. Appl. Math.*, **3** 28-41.
- Pilkington, M., 2009. 3D magnetic data-space inversion with sparseness constraints, *Geophysics*, **74**, L7-L15.
- Portniaguine, O. & Zhdanov, M. S., 1999. Focusing geophysical inversion images, *Geophysics*, **64**, 874-887
- Renaut, R. A., Vatankehah, S. & Ardestani, V. E., 2017. Hybrid and iteratively reweighted regularization by unbiased predictive risk and weighted GCV for projected systems, *SIAM J. Sci. Comput.*, **39(2)**, B221-B243.
- Vatankehah, S., Ardestani, V. E. & Renaut, R. A., 2014. Automatic estimation of the regularization parameter in 2-D focusing gravity inversion: application of the method to the Safo manganese mine in northwest of Iran, *Journal Of Geophysics and Engineering*, **11**, 045001.
- Vatankehah, S., Ardestani, V. E. & Renaut, R. A., 2015. Application of the χ^2 principle and unbiased predictive risk estimator for determining the regularization parameter in 3D focusing gravity inversion, *Geophys. J. Int.*, **200**, 265-277.
- Vatankehah, S., Renaut, R. A. & Ardestani, V. E., 2017a. 3-D Projected L_1 inversion of gravity data using truncated unbiased predictive risk estimator for regularization parameter estimation, *Geophys. J. Int.*, **210(3)**, 1872-1887.
- Vatankehah, S., Renaut, R. A. & Ardestani, V. E., 2017b. A fast algorithm for regularized focused 3-D inversion of gravity data using the randomized SVD, *Submitted to Geophysics*, arXiv:1706.06141v1
- Vogel, C. R., 2002. *Computational Methods for Inverse Problems*, SIAM Frontiers in Applied Mathematics, SIAM Philadelphia U.S.A.
- Voronin, S., Mikesell, D. & Nolet, G., 2015. Compression approaches for the regularized solutions of linear systems from large-scale inverse problems, *Int. J. Geomath*, **6**, 251-294.
- Wei, Y., Xie, P. & Zhang, L., 2016. Tikhonov regularization and randomized GSVD, *SIAM J. Matrix Anal. Appl.*, **37(2)**, 649-675.
- Wohlberg, B. & Rodríguez, P. 2007. An iteratively reweighted norm algorithm for minimization of total variation

functionals, *IEEE Signal Processing Letters*, **14** (12), 948–951.

Xiang, H. & Zou, J. 2013. Regularization with randomized SVD for large-scale discrete inverse problems, *Inverse Problems*, **29**, 085008.

Xiang, H. & Zou, J. 2013. Randomized algorithms for large-scale inverse problems with general Tikhonov regularization, *Inverse Problems*, **31**, 085008.

APPENDIX A: THE GENERALIZED SINGULAR VALUE DECOMPOSITION

Suppose $\tilde{G} \in \mathcal{R}^{m \times n}$, $\tilde{D} \in \mathcal{R}^{p \times n}$ and $\mathcal{N}(\tilde{G}) \cap \mathcal{N}(\tilde{D}) = 0$, where $\mathcal{N}(\tilde{G})$ is the null space of matrix \tilde{G} . Then there exist orthogonal matrices $U \in \mathcal{R}^{m \times m}$, $V \in \mathcal{R}^{p \times p}$ and a nonsingular matrix $X \in \mathcal{R}^{n \times n}$ such that $\tilde{G} = U\Lambda X^T$ and $\tilde{D} = VMX^T$ (warning Citation ‘PaSa:1981’ on page 19 undefined; Aster et al. 2013). Here, $\Lambda \in \mathcal{R}^{m \times n}$ is zero except for entries $0 < \Lambda_{1,(n-m)+1} \leq \dots \Lambda_{m,n} < 1$, and M is diagonal of size $p \times n$ with entries $M_{1,1} > M_{2,2} \geq \dots \geq M_{p^*,p^*} > 0$, where $p^* := \min(p, n)$. The generalized singular values of the matrix pair $[\tilde{G}, \tilde{D}]$ are $\gamma_i = \lambda_i/\mu_i$, where $\gamma_1 = \dots = \gamma_{(n-m)} = 0 < \gamma_{(n-m)+1} \leq \dots \leq \gamma_n$, and $\Lambda^T \Lambda = \text{diag}(0, \dots, 0, \lambda_{(n-m)+1}^2, \dots, \lambda_n^2)$, $M^T M = \text{diag}(1, \dots, 1, \mu_{(n-m)+1}^2, \dots, \mu_n^2)$, and $\lambda_i^2 + \mu_i^2 = 1, \forall i = 1 : n$, i.e. $M^T M + \Lambda^T \Lambda = I_n$.

Using the GSVD, introducing \mathbf{u}_i as the i th column of matrix U , we may immediately write the solution of (9) as

$$\mathbf{h}(\alpha) = \sum_{i=(n-m)+1}^n \frac{\gamma_i^2}{\gamma_i^2 + \alpha^2} \frac{\mathbf{u}_{i-(n-m)}^T \tilde{\mathbf{r}}}{\lambda_i} (X^T)_i^{-1}, \quad (\text{A.1})$$

where $(X^T)_i^{-1}$ is the i th column of the inverse of the matrix X^T .